Bio-Design and Manufacturing (2024) 7:167–180
https://doi.org/10.1007/s42242-023-00268-w

RESEARCH ARTICLE

Wearable multilead ECG sensing systems using on-skin stretchable and breathable dry adhesives

Yingxi Xie[1] · Longsheng Lu[1] · Wentao Wang[2] · Huan Ma[3]

Received: 4 August 2023 / Accepted: 29 December 2023 / Published online: 25 February 2024

Abstract

Electrocardiogram (ECG) monitoring is used to diagnose cardiovascular diseases, for which wearable electronics have attracted much attention due to their lightweight, comfort, and long-term use. This study developed a wearable multilead ECG sensing system with on-skin stretchable and conductive silver (Ag)-coated fiber/silicone (AgCF-S) dry adhesives. Tangential and normal adhesion to pigskin (0.43 and 0.20 N/cm^2, respectively) was optimized by the active control of fiber density and mixing ratio, resulting in close contact in the electrode–skin interface. The breathable AgCF-S dry electrode was nonallergenic after continuous fit for 24 h and can be reused/cleaned (>100 times) without loss of adhesion. The AgCF encapsulated inside silicone elastomers was overlapped to construct a dynamic network under repeated stretching (10% strain) and bending (90°) deformations, enabling small intrinsic impedance (0.3 Ω, 0.1 Hz) and contact impedance variation (0.7 kΩ) in high-frequency vibration (70 Hz). All hard/soft modules of the multilead ECG system were integrated into lightweight clothing and equipped with wireless transmission for signal visualization. By synchronous acquisition of I–III, aVR, aVL, aVF, and V4 lead data, the multilead ECG sensing system was suitable for various scenarios, such as exercise, rest, and sleep, with extremely high signal-to-noise ratios.

Graphic abstract

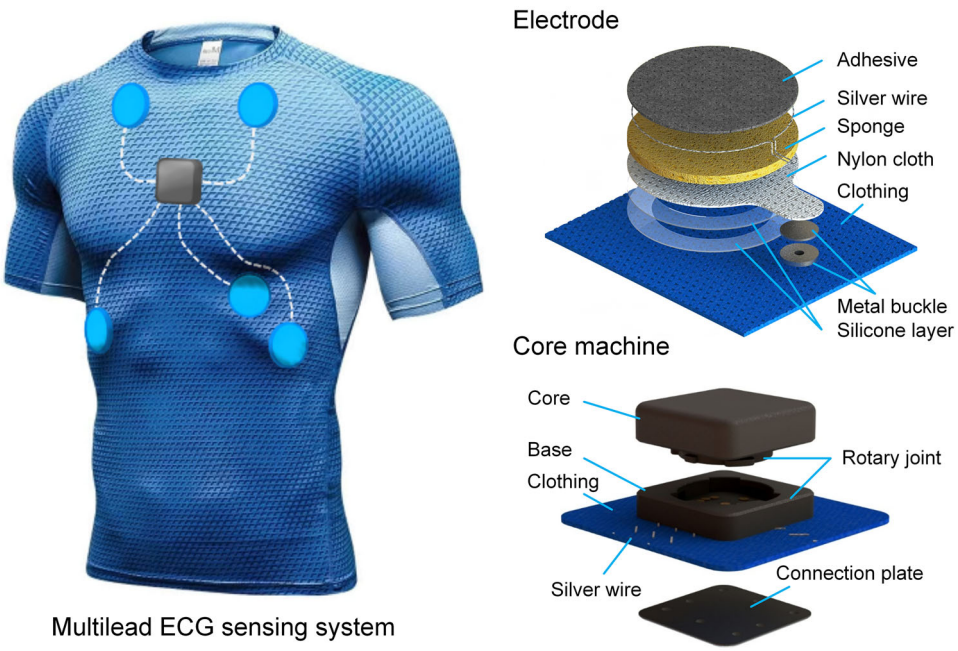

Keywords Multilead electrocardiogram · Dry electrodes · Wearable electronics · Wireless transmission

Introduction

Cardiovascular diseases (CVDs) are the leading cause of death in today's aging society [1]. The early diagnosis of these diseases relies on the electrocardiogram (ECG), a valuable tool for the noninvasive monitoring of cardiac potential [2–4]. Because ECG devices used in hospitals and clinics are rigid, boxy, and incapable of 24/7 measurements [5, 6], the pursuit of efficient solutions that enable continuous cardiac monitoring out-of-hospital is becoming a hot topic [7, 8]. Wearable ECG sensing systems with thin, soft, and skin-attachable patches could be worn and washed regularly, providing comfortable and long-term use experiences [9]. Not only can they conform to nonplanar and dynamic human skin, but they also provide an ideal platform for integration into everyday objects, such as clothing, seats, or hospital beds [10].

In the traditional wearable ECG sensing systems, all active components comprised of rigid silicone integrated circuits (ICs). These devices are often encapsulated into fabrics with an elastic layer to realize specific functions, but user comfort is severely reduced [11–14]. Another wearable ECG device that uses all units is flexible for the human body; however, it has a limited lifespan because of poor mechanical properties [15, 16]. As a compromise, wearable ECG devices with front-end components based on soft elastomer and brittle ICs used for the rest of the system are now mainstream [17]. This system has a rigid-flexible balance of mechanical properties, in which on-skin stretchable ECG electrodes are a key factor of the human–machine interface [18–21]. Nowadays, silver/silver chloride (Ag/AgCl) gel electrodes are commonly used in ECG clinical monitoring, but they have disadvantages such as skin irritation and short service life [22–24]. Therefore, many dry electrodes with the same diagnostic efficiency as Ag/AgCl gel electrodes are employed for continuous ECG monitoring [25, 26]. Nevertheless, signals collected by on-skin dry electrodes are often of low quality, especially in dynamic environments, due to the high impedance of the follow-up skin and lack of adhesive [27].

To address the former limitation, various attempts have been made to manufacture on-skin ECG electrodes, such as elastic nanocomposites consisting of Ag nanowires (AgNWs), Ag nanoparticles (AgNPs), graphene, and carbon nanotubes (CNTs), or to design shape-adaptive wavy, cellular, helical, and spring-like geometries [28–31]. Jung et al. [32] manufactured a CNT/polydimethylsiloxane (PDMS) dry ECG electrode that could be attached under dry/wet conditions. Qin et al. [33] fabricated a AgNW-based ECG dry electrode to collect stable signals in sitting/walking situations. For the second issue, ECG electrodes must be highly durable and nonirritating to the human skin [22, 34]. Kim et al. [28] reported a gecko-like structure composed of high-aspect-ratio micropillars and nanorods that repeatedly adhere to the skin. The above-mentioned studies have done a good job of fabricating ECG dry electrodes. Unfortunately, most of them focus on material preparation or sensing performance, and it would be better to further explore the resistance, adhesion, and breathability of on-skin electrodes in combination with back-end applications [35–37].

To advance the cutting-edge wearable ECG sensing systems exclusively based on flexible electronics, this study reported an on-skin stretchable, breathable, and conductive dry adhesive using Ag-coated fiber/silicone (AgCF-S) for wearable multilead ECG devices. AgCFs were first made into a fiber mat by wet-hair-laying craft and encapsulated with a hybrid silicone-based elastomer composed of Ecoflex and silicone gel. Microholes were laser drilled on the silicone-based substrate for great air permeability. High normal and tangential adhesion was obtained with 95.8% retention after 100 manual reuses. Under repeated stretching and bending deformations, AgCFs overlapped into a dynamic conductive network with small intrinsic and contact impedances. In combination with self-developed ICs for signal acquisition, amplification, and digitization, the wearable ECG device could capture I–III, aVR, aVL, aVF, and V4 lead data with high signal-to-noise ratios (SNRs) and could be visualized on a mobile terminal.

Experiments

Materials and processing parameters

AgCFs (resistance: about 10 Ω/cm; tensile strength: about 5.8 GPa; Ag content: about 18% (mass fraction); diameter: 15–20 μm; density: 3.34 g/cm^3) (JLSUN Textile Co., Ltd., China) with 2, 3, 4, and 5 mm length were mixed with ethanol and stirred evenly to form a suspension (Fig. 1). The AgCF suspension was extracted by vacuum and flowed to the steel mesh to form a wet mat. The fiber mat was pressed, dehydrated, and dried in an oven at 60 °C for 1 h. Silicone rubber (Ecoflex, Smooth-on 0030, Smooth-On Inc., USA) was prepared by mixing A and B components (1:1 mass ratio). Silicone gel (QGEL300, Topgun Glue Co., Ltd., China) was added to Ecoflex at different ratios from 50% to 80% and stirred into an elastomer. For convenience, the sample codes were defined according to the mass ratio of Ecoflex to silicone gel. The fiber mat was pressed under the machine with a pressure of 10 MPa. The mixed silicone gel was added to the mat and cured at 70 °C for 1 h to prepare a AgCF-S dry adhesive. Laser drilling of the AgCF-S dry adhesive was carried out with a pulsed ultraviolet (UV) laser system (λ=355 nm; Macro Blue Electric Technology Co., Ltd., China). The maximum value of the UV laser beam was 10 W, and the minimum

Extended author information available on the last page of the article

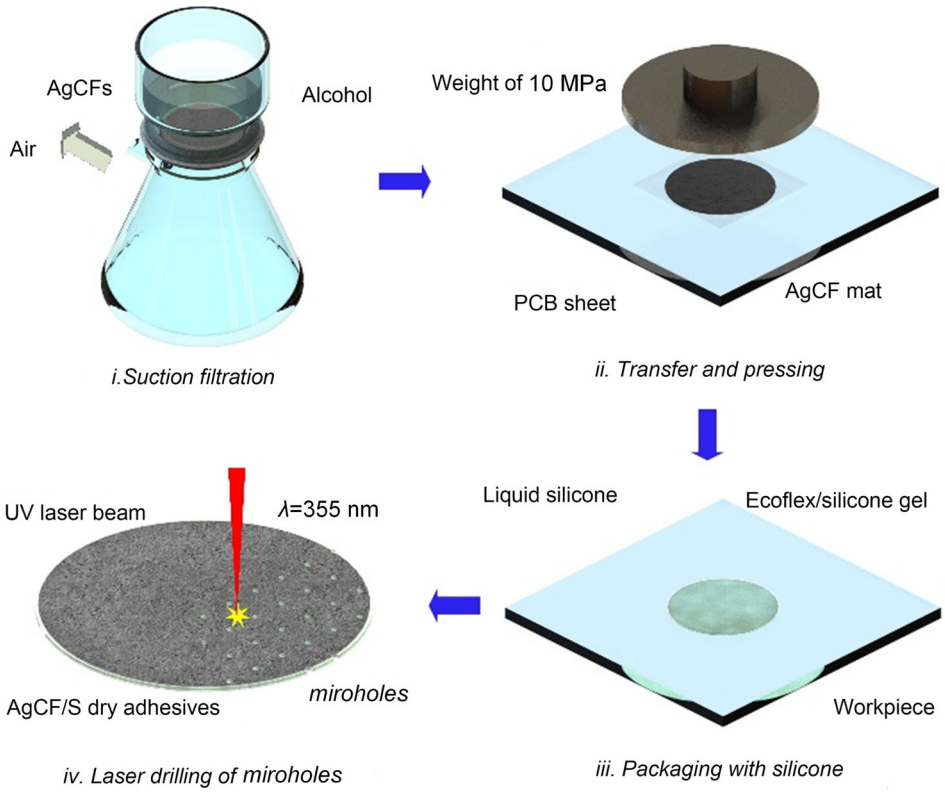

Fig. 1 Schematic diagram of the manufacturing process of AgCF-S dry adhesives. AgCF-S: silver-coated fiber/silicone; PCB: printed circuit board; UV: ultraviolet

diameter of the spot was about 20 μm. Microholes on the AgCF-S dry adhesive were made using a dot-matrix pattern with a scan interval of 1 mm, laser power of 2 W, scan rate of 100 mm/s, and frequency of 20 kHz.

Characterization

A field-emission scanning electron microscopy (SEM; Zeiss Merlin, Germany) was used to investigate surface/cross-section morphologies. Thermal gravimetric analysis (TGA; STA 449C) was performed from room temperature to 800 °C at a heating rate of 10 °C/min in air. X-ray photoelectron spectroscopy (XPS; Quantera SXM, PHI) was done with a base pressure of 5×10^{-9} Torr (1 Torr=133.3 Pa). Fourier transform infrared (FT-IR) spectra were recorded (Bruker Vertex 70, Germany) with a wavenumber range of 400–4000 cm^{-1} at a resolution of 4 cm^{-1}. SEM, FT-IR, and XPS characterizations were conducted directly on ECG electrodes.

Sheet resistance was measured by a four-point conductive meter (RC3175, EDTM) in five different locations. A self-built dynamic frequency impedance device was powered by a digital source meter (CC2450; Keithley, USA). The vibration was recorded by a triaxial force sensor (GSV-4; ME-Messsysteme, Germany). Impedance measurement was done by inductance resistance and capacitance (LCR) digital bridge (TH2838; Tonghui, China). Adhesion was tested on a tensile testing machine (ZQ-990B; Zhizhi Company, China) with data recorded by a high-precision force sensor (GSV-4; ME-Messsysteme). The AgCF-S dry adhesive was cut to the appropriate size, the adhesion area was 1 cm×1 cm, and 10 kPa pressure was applied during adhesion and removed to make it completely fit on the surface. During the test, tangential displacement was applied at a speed of 5 mm/min to test the tangential adhesion force, and the sample was peeled off at 90° from the adhesive object at a normal speed of 5 mm/min.

Integration of the wireless sensing system

Integration of AgCF-S dry adhesives with the wireless sensor system was completely self-designed. The circuit was divided into main and base circuits; both were built on a printed circuit board (PCB; JLC Electronics, China) with analog acquisition, conversion, and wireless transmission functions. The hardware was controlled by a microcontroller (STM8L151; STMicroelectronics, Italy), and the ECG signal was processed by an ECG front-end (ADS1293; Texas Instruments, USA). ECG data were transmitted by Bluetooth (HJ-131; Hongjia Electronic Technology, China) and read by a mobile client. Fifty volunteers participated in data collection, and four segments of data were collected in different scenes, each lasting 20 s. Wearable sensing measurements

did not involve any ethical animal experiments. Experiments involving human subjects were conducted with the full informed consent of volunteers.

Results and discussion

Concept and assembly of wearable ECG sensing systems

Long-time monitoring of CVDs has been the focus of research. In Fig. 2a, the self-adhesive ECG sensor wirelessly transmits physiological data while a person is running, thus playing a role in health monitoring [38]. This study designed a wearable multilead ECG sensing system that relies on the principle of biopotential acquisition, consisting of three main modules: the core machine, ECG dry electrodes, and clothing (Fig. 2b). ECG electrodes attached to the human skin could provide a low contact impedance for voltage reading. Clothing is combined with the ECG sensing system and used as an everyday item. The core machine converts health data with high SNR for wireless transmission or further signal processing for disease prevention. Three factors were considered for the assembly of the multilead ECG sensing system: (1) softness and flexibility for user comfort, (2) stable mechanical strength integrated with clothing, and (3) easy access to backend hardware [39, 40].

The ECG electrode is an important part of the human—machine interface connecting soft skin and the rigid core machine. Figure 2c shows the layer-by-layer schematic illustration of ECG dry electrodes, where the cross-sectional assembly is divided into three parts. The dry adhesive on top is firmly attached to the human skin to collect ECG signals. As a transition from flexible to rigid, two layers of sponge and nylon are used in the middle and bottom, respectively. The sponge relieves stress, absorbs sweat, and keeps the surface dry to recognize bioelectrical signals. The nylon substrate prevents the ECG dry adhesive from being torn. A small amount of Ecoflex seals the gap between each layer. Ag wires are embedded in AgCF-S adhesives to form electrical connections.

Preparation and characterization of wearable ECG electrodes

Dry electrodes are key to addressing the limitations of ECG sensors in harsh operating environments, including stretching, twisting, and folding [41]. Therefore, using the concept of paper fabrication and laser drilling, an ultralight and flexible ECG dry adhesive is prepared [42]. In Fig. 3a, the placement of the AgCF-S dry adhesive (density about 1.22 mg/mm^3) on the flower does not affect its normal posture. Due to good adhesion under dry/wet conditions, the AgCF-S dry adhesive is attached to hand without affecting the normal deformation of skin (Fig. 3b). The AgCF-S dry adhesive can also be folded freely into crafts and placed above hot gas without affecting the natural ascent of gas flow (Fig. 3c). The above results provide a promising prospect for the use of flexible, lightweight, and breathable AgCF-S dry adhesive in wearable ECG sensing systems (Fig. 3d).

The surface morphology of the AgCF-S dry adhesive is shown in Fig. 3e, where the high-density conductive network is responsible for bioelectric collection. The enlarged image demonstrates that the nodes between AgCFs are wrapped by silicone-based elastomers, making ECG dry electrodes mechanically stable. The AgCF-S dry adhesive is punched (interval distance of about 1 cm) without affecting the integrity of the soft substrate (Fig. 3f). The cross-section morphology displays microholes (diameter about 100 μm and deepness about 320 μm) throughout the entire electrode (Fig. 3g). The electrode should be fully designed to establish an electrical connection with the skin. To make this clearer, a diagram (Fig. S1 in Supplementary Information) is drawn to show how adhesion and electrical connections are balanced. The whole electrode is not sandwiched, and the AgCF part is exposed to the outside, which can achieve good adhesion to the skin, and there is a large amount of silica gel on the surface that can play a role in adhesion. In Fig. 3h, the close bonding between AgCF and the elastic substrate is beneficial to the dynamic mechanical and electrical stability, thus prolonging the service life of the AgCF-S dry adhesive.

Element mapping results show that the structure of AgCF is stable after being encapsulated by a silicone-based elastomer (Fig. 3i). FT-IR spectra of pure AgCF and AgCF-S dry adhesives are displayed in Fig. S2 (Supplementary Information). Peaks at 784.4, 1007.7, and 1257.3 cm^{-1} are attributed to the stretching vibration absorption of Si–O, Si–C, and Si–CH_3, respectively. The thermal stability of pure AgCF and AgCF-S dry adhesives is confirmed by TGA (Fig. S3 in Supplementary Information). From the beginning, the dehydration reaction takes place inside the silicone gel and completes at about 99.3 °C. The carbonization of nylon starts at about 310.3 °C, and the incomplete amorphous carbon continues to react with oxygen in airflow. Only a part of the Ag component remains when the temperature increases to about 508.1 °C. Furthermore, the residual Ag content of the AgCF-S dry adhesive is about 17.5%, lower than that of pure AgCF. The surface composition of the AgCF-S dry adhesive is investigated by full XPS spectra in Fig. S4 (Supplementary Information). Detection of a small amount of Ag indicates that the package of AgCFs in silicone-based elastomer is intact (Fig. S5 in Supplementary Information).

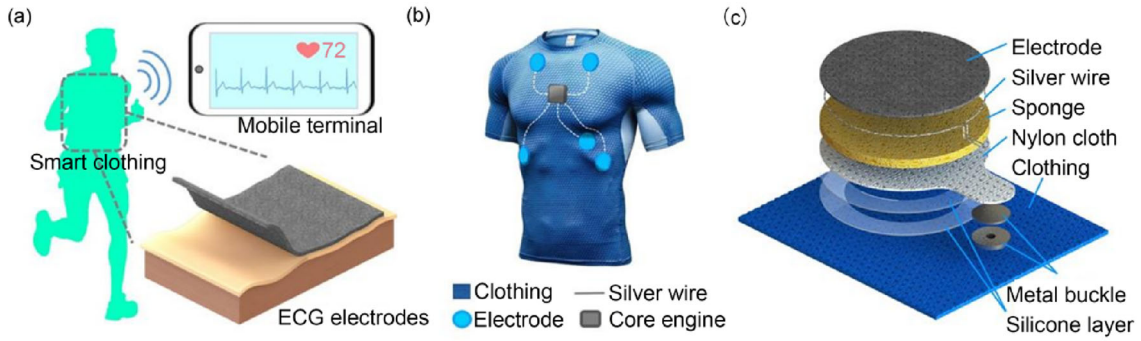

Fig. 2 **a** Schematic diagram of the wearable ECG sensing system for real-time human health monitoring. **b** Schematic diagram of the multi-lead ECG sensing system consisting of three modules: the core machine, ECG dry electrodes, and clothing. **c** Layer-by-layer diagram of a single ECG dry electrode. ECG: electrocardiogram

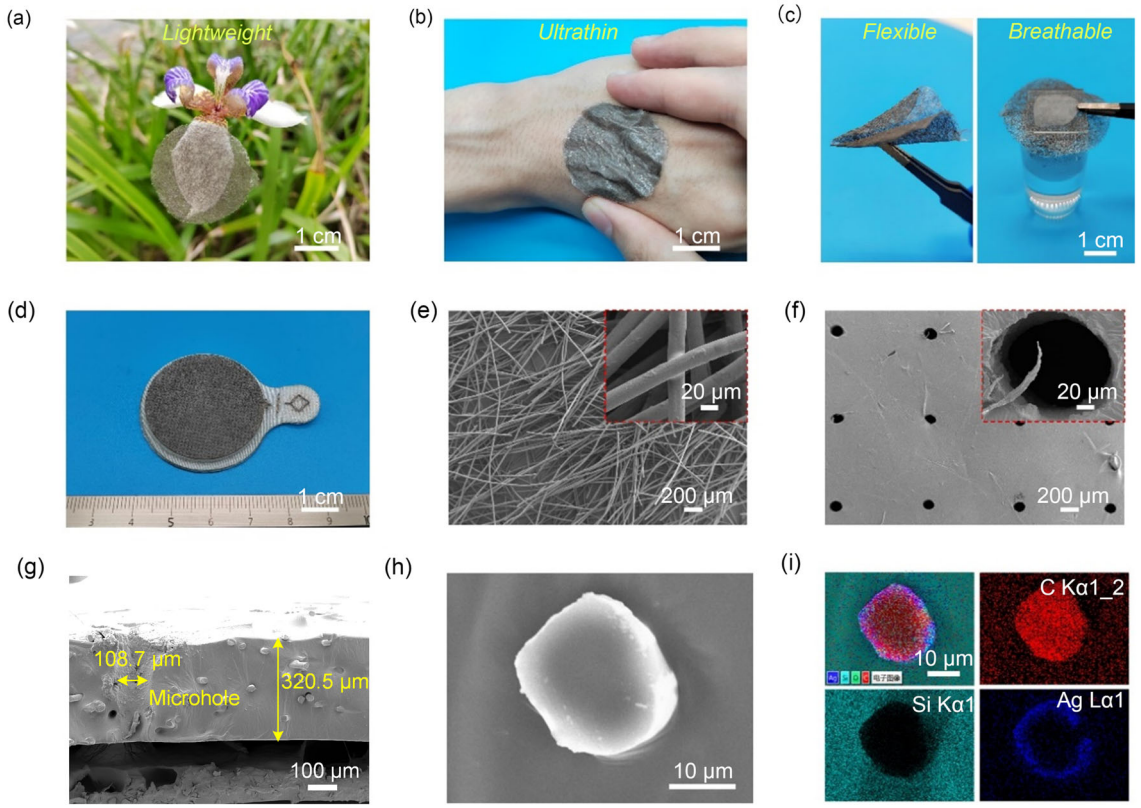

Fig. 3 **a** Lightweight, ultrathin, and flexible features of the AgCF-S dry adhesive are demonstrated by staying on the flower. **b** The AgCF-S dry adhesive is adhered to the hand, and **c** folded into an airplane and permeated in thermal airflow. **d** Optical image of the ECG dry electrode. **e** SEM image of AgCFs. The enlarged view shows that the nodes are connected by a silicone elastomer. **f** SEM image of the AgCF-S dry adhesive and its periodic microholes. **g** Cross-section morphology of laser-drilled microholes. **h** Enlarged SEM image of a AgCF embedded in the elastomer. **i** Element mapping results. AgCF-S: silver-coated fiber/silicone; ECG: electrocardiogram; SEM: scanning electron microscopy

Adhesion and electrical properties of wearable ECG electrodes

To investigate the tensile and conductive properties of ECG electrodes, AgCF-S dry adhesives with different fiber densities were prepared. In Fig. 4a, with increasing surface densities from 8.8 to 35.2 g/m^2, the sheet resistance of AgCF-S dry adhesives (top and bottom layers) decreased linearly and reached a minimum value of 1.37 Ω/sq. However, the elongation of AgCF-S electrodes was sacrificed due to the increase in rigidity (Fig. 4b). During loading/unloading at 10% strain (>2000 cycles), the AgCF-S dry adhesive illustrated good resistance stability at an areal density of 26.4 g/m^2 (Fig. 4c). The resistive response of AgCF-S dry adhesives was still stable over 2000 cycles at the bending deformation at 90°, with small retention of about 10.7% (Fig. S6 in Supplementary Information). Due to the strong interfacial bonding between AgCFs and silicone-based elastomers, great mechanical stability was obtained without sacrificing electrical conductivity. The AgCF-S dry adhesive also demonstrated a great recovery ability in a single stretching/bending circle (Fig. S7 in Supplementary Information). From the philosophy of the rigid-flexible balance, a AgCF-S dry adhesive (areal density of 26.40 g/m^2) with moderate tensile strength (0.12 MPa) and elongation (56.7%) was adopted as the object of follow-up research. Electrical and mechanical hysteresis curves at maximum tensile stress also indicate relatively small resistance fluctuations and good resilience of the electrode, thus assuring ECG testing under extreme conditions (Fig. S8 in Supplementary Information). Adhesion of ECG dry electrodes is very significant for bioelectrical signal acquisition. As shown in Fig. 4d, a pigskin was placed on the as-prepared AgCF-S dry adhesive, with a force sensor installed at the bottom. The platform was adjusted to 180° and 90° for tangential and normal adhesion tests, respectively. Ecoflex/silicone gel with different mixing ratios tunes the adhesion properties. Due to the inherent stiffness of Ecoflex, tangential adhesion and elongation first increased and then decreased with decreasing silicone ratios (Fig. 4e). In the normal adhesion test, there was no difference in displacement because of slope setting, whereas maximum stress increased with the increase in silicone gel content (Fig. 4f). Adhesion was optimized at the Ecoflex/silicone ratio of 3:7 (E3S7) with high tangential and normal values of 0.43 and 0.20 N/cm^2, respectively.

As mentioned above, commercial Ag/AgCl gel electrodes have a limited lifespan and cannot be reused in long-term ECG monitoring. Therefore, the AgCF-S dry electrode was improved in terms of repeatability and reliability. In Fig. S9 (Supplementary Information), AgCF-S electrodes show good tangential and normal adhesion even on wet pigskins, making them suitable for testing on a sweaty body. In Fig. 4g, the as-prepared ECG dry electrode was not damaged and only had some dust after repeated use. The function and shape of AgCF-S dry electrodes were well-preserved after 100 washes and repeated use, and the retention of adhesion and increase of conductivity are listed in Figs. 4h and 4i, respectively. Adhesion of the AgCF-S dry electrode decreased to 40.1% after repeated use, whereas it remained at 95.8% after washing. The silicone layer outside of AgCFs isolates the incoming water and withstands extreme conditions such as high temperature and external forces. Whether the ECG electrode was repeatedly used or washed, its resistance was relatively stable, with a small decrease of 6.2% and 2.1%, respectively.

The experimental setup of intrinsic/contact impedance stability under dynamic frequency is shown in Figs. 5a–5c. Using a rotary vibration motor to provide external vibration, the impedance–time curve was recorded by a force sensor and output to the computer. Two electrodes were formed with a "sandwich" structure. The top electrode was a copper foil with a vibration motor on it. The bottom electrode was electrically connected to the sample under test. In Figs. 5d–5g, the intrinsic impedance of pure AgCF and AgCF-S dry electrodes has small values in the frequency range of 0.01–100 Hz. The impedance angle close to 0° proves that they have almost pure resistance. By comparing the contact impedance of specific frequencies, including 1, 100, and 1000 Hz, and the ratio of the contact impedance to the thickness, the intrinsic impedance of the 3M gel electrode was larger but its contact impedance was smaller at all the three frequencies (Fig. S10 in Supplementary Information). The overall contact impedance changed little after 100 reuses at a larger frequency of 100–1000 Hz (Fig. S11 in Supplementary Information). According to the dry/wet ECG electrode circuit model, the hydrogel is equivalent to a resistor. Changes in impedance angle and intrinsic impedance come from two aspects: (1) oxidation and/or reduction reactions at the interface between the copper foil and electrolyte, and (2) phase angle impedance between the resistance and electrolyte. The contact impedance of the AgCF-S dry adhesive is larger than that of pure AgCF, but impedance angles are similar due to contact capacitance. The contact interface is described as an impedance in parallel with a resistor and a capacitor by the following formula:

$$Z = \frac{R}{1 + \mathrm{j}2\pi f RC}, \tag{1}$$

where Z is the contact impedance, R is the contact resistance, C is the contact capacitance, f is the frequency, and j is the imaginary part. The lower resistance of the AgCF-S dry electrode and its good interfacial adhesion favor a relatively low contact impedance. In Fig. 5h, 3M and AgCF-S dry electrodes kept the bonding shapes under a hanging weight of 10 g, but the pure AgCF detached from the pigskin. Under

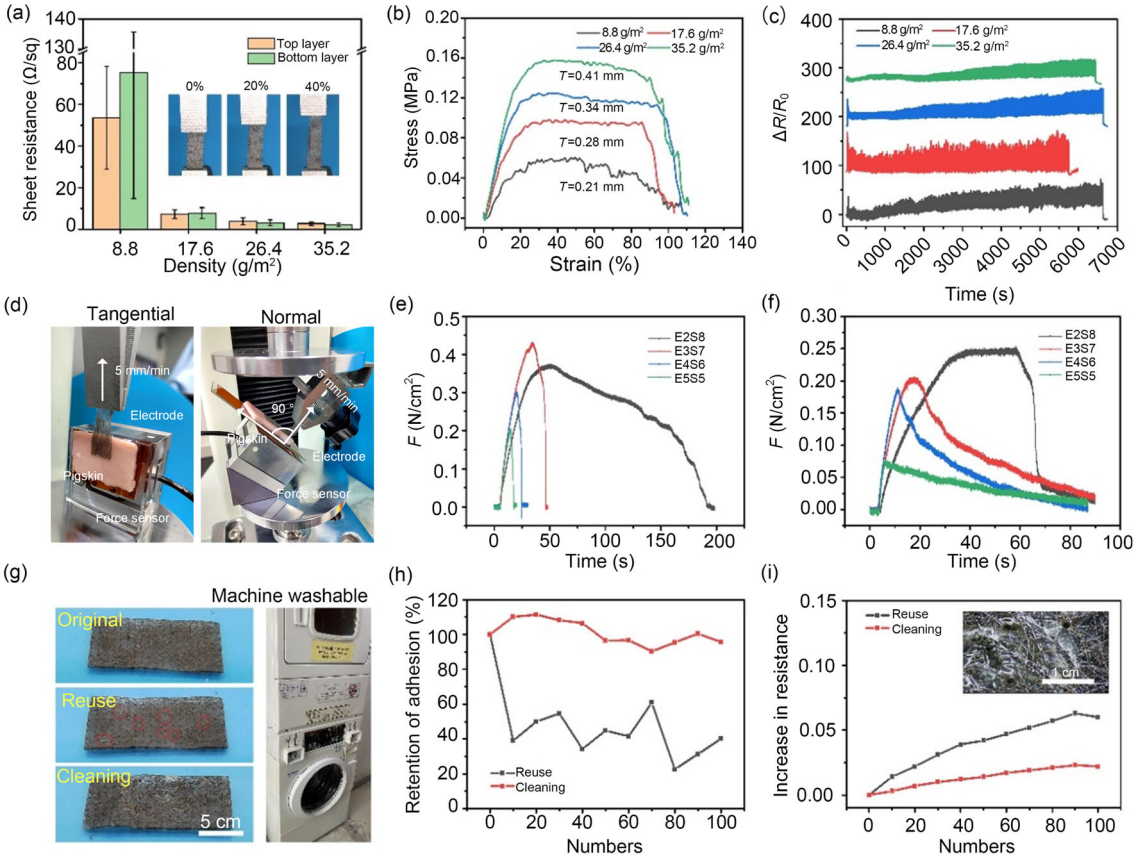

Fig. 4 **a** Sheet resistance of AgCF-S dry electrodes at surface densities of 8.8, 17.6, 26.4, and 35.2 g/m^2. **b** Strain–stress curves and **c** resistance stability of AgCF-S dry electrodes. **d** Experimental setting of AgCF-S dry electrodes in tangential and normal adhesion measurements. **e**, **f** Adhesion force as a function of time in **e** tangential and **f** normal stretching tests (E2S8, E3S7, E4S6, and E5S5 stand for Ecoflex/silicone mass ratios of 2:8, 3:7, 4:6, and 5:5, respectively). **g** Optical images of AgCF-S dry electrodes after 100 times of reusing and washing (left) and the washing process (right). **h** Adhesion retention and **i** resistance increase of AgCF-S dry electrodes. AgCF-S: silver-coated fiber/silicone

dynamic vibration, the impedance variation of the AgCF-S dry electrode was smaller than that of the pure AgCF electrode but larger than that of the 3M electrode (Fig. 5i). The stability of contact impedance plays an important role in signal detection. Figure 5j shows a sinusoidal waveform of the AgCF-S dry electrode at about 70 Hz, indicating its good stability to work under extreme conditions. The ECG dry electrode with high water vapor permeability is an ideal choice for on-skin sensing applications, allowing the rapid evaporation of sweat from the human body. After AgCF-S dry electrodes were worn on the human body for 24 h, the human skin showed no redness based on imaging results (Fig. S12 in Supplementary Information). Therefore, breathable ECG electrodes could reduce the risk of inflammation. In Fig. 5k, samples were attached to bottles containing pure water to study water evaporation at 27 °C. Based on pigskin, the mark of AgCF-S electrodes left on the pigskin was the lightest after 24 h bonding relative to 3M gel and pure AgCF electrodes (Fig. 5l).

In Fig. 5m, the water vapor permeability of 3M gel, pure AgCF, and AgCF-S dry electrodes is 0.2, 7.3, and 2.7 mg/(cm^2·h), respectively. The water permeability of the AgCF-S dry electrode is about 12 times higher than that of the 3M gel electrode. Although the gas permeability of pure AgCF is the largest, it cannot be normally attached to the skin. Therefore, compared to 3M gel and pure AgCF electrodes, the AgCF-S dry electrode shows balanced performance in terms of mechanical properties, adhesion, and air permeability.

Integrated design of the multilead ECG sensing system

Integrating a multilead ECG system into a commercial garment with a three-lead layout is lightweight and comfortable and does not cause negative effects. Commercial clothing is tight and can give the ECG electrode force against the skin, partially compensating for the decline in adhesion

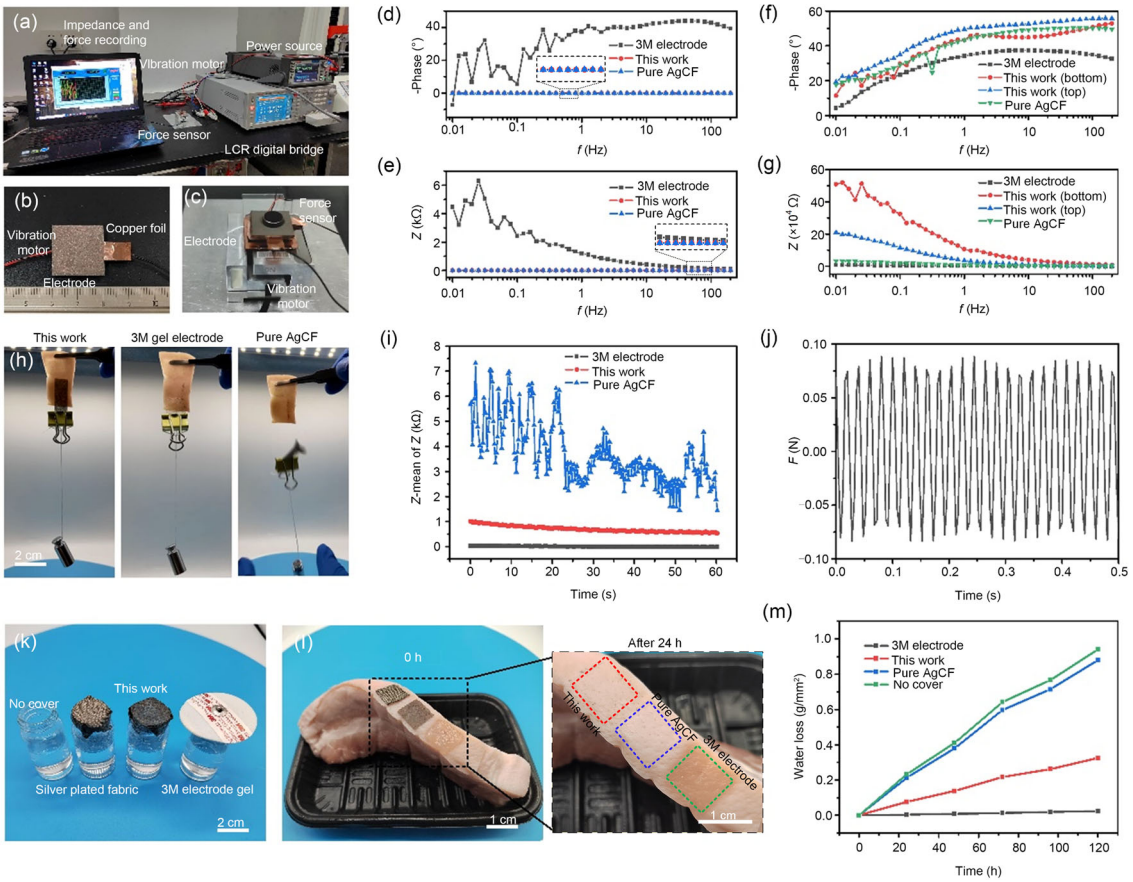

Fig. 5 **a**–**c** Experimental setup for impedance stability testing at dynamic frequencies. **d**, **e** Intrinsic phase and impedance and **f**, **g** contact phase and impedance of 3M gel, pure AgCF, and AgCF-S dry electrodes in the 0.01–100 Hz frequency range. **h** Three electrodes are attached to pigskin with 10 g weight. **i** Variation in contact impedance of 3M gel, pure AgCF, and AgCF-S dry electrodes on pigskin. **j** Enlarged impedance at dynamic vibration of about 70 Hz. **k** Commercial 3M gel, pure AgCF, and AgCF-S dry electrodes are covered on bottles containing water and **l** attached to pigskin for 24 h to estimate water evaporation. **m** Water vapor permeability within 120 h. AgCF-S: silver-coated fiber/silicone

after repeated use. The hardware architecture is illustrated in Fig. 6a. The front-end chip of the ECG system is ADS1293, which communicates with the microcontroller unit (MCU) through a serial peripheral interface (SPI). The I–III signals obtained from RA (right arm), LA (left arm), and LL (left leg) leads are given by [14]

$$\mathrm{I} = \mathrm{LA} - \mathrm{RA}, \tag{2}$$

$$\mathrm{II} = \mathrm{LL} - \mathrm{RA}, \tag{3}$$

$$\mathrm{III} = \mathrm{II} - \mathrm{I}, \tag{4}$$

where the operations of I and II leads are realized by subtraction of the operational amplifier. After obtaining the above-mentioned signals, three pressurized leads (aVR, aVL, and aVF) are further calculated. RL is the driven-right-leg combined with the IC to suppress common-mode signals.

The gain of the driven-right-leg needs to be increased based on a typical value; thus, the Wilson reference potential is obtained from biopotentials of RA, LA, RL (right leg), LL, and V4 (chest) leads. The IC chip interacts with the MCU via an SPI. Because the signal levels are inconsistent with that of the MCU, a high-speed chip is employed for isolation. The N-type metal–oxide–semiconductor is used to control the conversion chip. Bluetooth is a low-power module packaged at the chip level and communicates with the MCU by a universal asynchronous receiver/transmitter interface. Different IC levels are provided by a low dropout regulator. The front-end chip transmits the digital signal to the MCU for packaging and sends it to Bluetooth for wireless transmission.

Removing the baseline is necessary to determine the severity of the ECG signal; otherwise, it is difficult to determine the heart disease. Thus, a simple wavelet transform based baseline removal function ("db4" wavelet, sixth-order

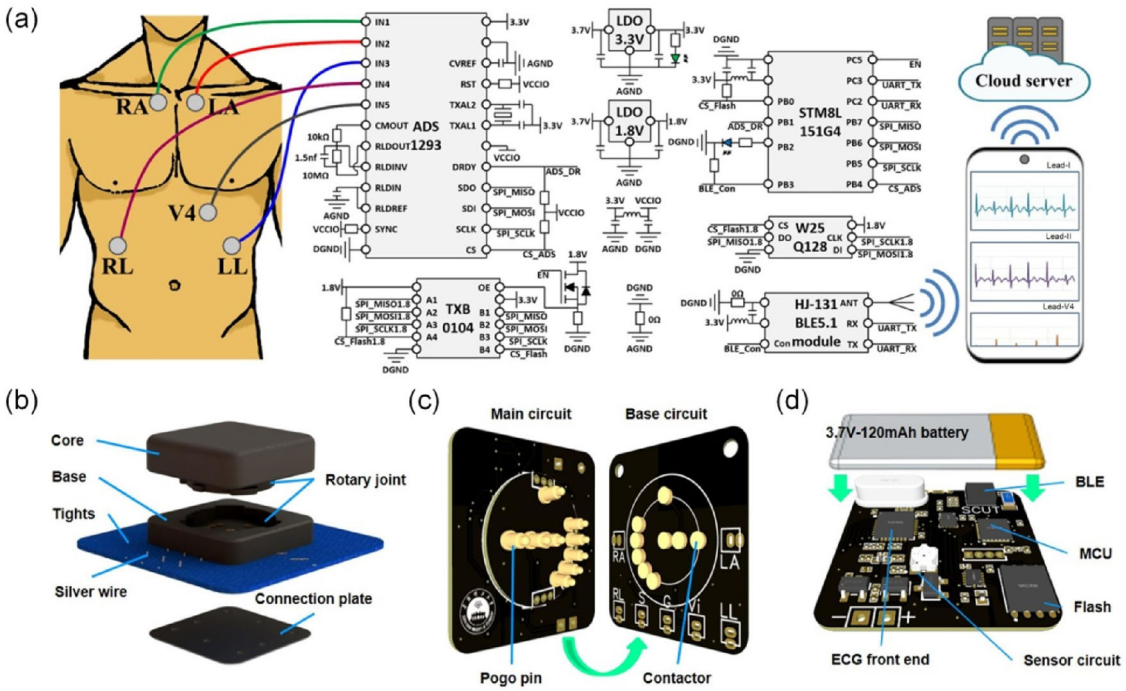

Fig. 6 **a** Hardware design of the IC. ECG signals are displayed by the WeChat program and uploaded to the cloud server for storage. **b** Layer-by-layer schematic diagram of the ECG device. **c** Schematic diagram of the pogo pins and contactors on PCB. **d** Schematic diagram of the circuit layout on the core. IC: integrated circuit; ECG: electrocardiogram; PCB: printed circuit board; MCU: microcontroller unit; BLE: Bluetooth low energy; RA: right arm; LA: left arm; RL: right leg; LL: left leg

decomposition) is deployed on the cloud server for the real-time invocation of the applet, which can be expressed by the following formulas [19]:

$$T_\varphi(0,\,0) = \frac{1}{\sqrt{N}} \sum_{x=0}^{N-1} f(x)\varphi^*(x), \tag{5}$$

$$T_\psi(j,\,k) = \frac{1}{\sqrt{N}} \sum_{x=0}^{N-1} f(x)\psi_{j,k}^*(x), \tag{6}$$

where x is the discrete signal point, $f(x)$ is the discrete signal, N is the number of discrete signal points, $\varphi^*(x)$ is the conjugate of scale function, $\Psi_{j,k}^*$ is the conjugate of wavelet basis function, $T_\varphi(0,0)$ is the approximation coefficient, and $T_\Psi(j,k)$ is the series of detailed coefficients. The coefficients, scale functions, and wavelet basis functions after the above decomposition are reconstructed with the following formula [8]:

$$f(x) = \frac{1}{\sqrt{N}}\left[T_\varphi(0,\,0)\varphi_{0,0}(x) + \sum_{J=0}^{J-1}\sum_{k=0}^{2j-1} T_\psi(j,\,k)\psi_{j,k}(x)\right], \tag{7}$$

where $T_\varphi(0,0)\varphi_{0,0}(x)$ is a zero sequence in reconstructing. Each wavelet basis function has a fixed decomposition amount for the convolution sequence. Decomposition and refactoring are implemented through convolution step by step.

Layer-by-layer schematic diagram of the ECG device is shown in Fig. 6b. By setting the sampling frequency and bandwidth of the front-end chip to 320 samples/s and 65 Hz, respectively, the acquisition frequency to the ECG signal is 160 samples/s. Therefore, the final system satisfies the recording of multilead ECG signals at a frequency range of 0.5–50 Hz. The common-mode rejection ratio is calculated as 102 dB at 100 Hz due to the amplifier circuit in the front-end. In Fig. 6c, the hardware design of the multilead ECG system consists of two parts: (1) a core machine with chips and circuits, and (2) a base for physical and electrical connections. Figure 6d shows the layout of a core circuit. A series voltage divider circuit is used for ECG electrodes. Considering the stability of the internal op-amp power supply, the ECG processing front-end chip uses a 3.7 V supply with a low-power ripple. The AgCF-S dry electrode has higher contact impedance and common-mode interference than the 3M gel electrode, so the suppression signal V_{RLD} output from the right leg drive amplifier can be expressed as

$$V_{\mathrm{RLD}} = -\frac{|Z|V_{\mathrm{CMOUT}} - (|Z| + R)V_{\mathrm{RLDREF}}}{R_1}, \tag{8}$$

where $|Z|$ is the modulus of the impedance of a 10-MΩ resistor in parallel with 1.5 nF, V_{CMOUT} and V_{RLDREF} are respectively the output and reference voltages generated in the chip, and R_1 and R are the electrode resistance and 10-kΩ resistor, respectively.

The total weight of the multilead ECG sensing system, including clothing, ECG dry electrodes, and the core, is about 150 g (Fig. S13 in Supplementary Information), lighter than many state-of-the-art works and not burdensome for users to wear [43, 44]. The flowchart of signal acquisition, processing, transmission, and visualization of the multilead ECG sensing system is displayed in Fig. S14 (Supplementary Information). When ECG is tested with the AgCF-S dry electrodes, data are sent to the internal register of the front-end chip to start the working process. After receiving the startup command, the hardware samples ECG data and transmits them to the WeChat applet on a mobile phone. When the storage time reaches 800 s (5 s per cycle), the hardware suspends sending, and the software parses each piece of signal into 24-bit original data. ECG data are sent to the WeChat applet through a transmission control protocol, and a real-time graph is stored in the database.

Application of the wireless sensing system

In Figs. 7a–7d, multilead ECG signals obtained by the AgCF-S dry electrodes are stable when the volunteer is sitting or standing. P waves, Q, R, and S complexes, and T waves could be identified with very high similarity. In Figs. 7e and 7f, when the volunteer is repeatedly squatting, the ECG signal quality is not much degraded. There is no baseline drift and hard-to-recognize features due to the close fit of AgCF-S dry electrodes against the body. Basic ECG signals can still be observed when the volunteer is lying (Figs. 7g and 7h). The robustness of the wearable multilead ECG system is better demonstrated by some simple movements outdoors (Fig. 7i). ECG signals show smooth baselines with little fluctuation and noise when the volunteer is walking on the ground, a slope, and stairs (Fig. 7j). AgCF-S dry electrodes produce high-quality ECG signals characterized by P, Q, R, S, and T waveforms. Compared to pure AgCF and 3M gel electrodes, Q, R, and S waves of the AgCF-S dry electrode have the highest peak values of 0.15, 1.6, and 0.8 mV at I, II, and V4 leads, respectively (Fig. 7k). The baseline of the ECG signal is relatively stable with high-fidelity peaks, saving a lot of work for signal processing. AgCF-S dry electrodes are also cleaned and redried 100 times to detect ECG signals. With the increase in cleaning and redrying times, the interface contact between the electrode and skin is weakened, and the signals are easily disturbed by electrode displacement, but the overall difference is insignificant (Fig. S15 in Supplementary Information). After repeated washing and drying, the SNR of the ECG signal remains stable (Fig. S16 in Supplementary Information). Relative to commercial 3M electrodes, such high resolution could provide more information about abnormalities associated with potential CVDs, including arrhythmias, hypertrophy, and ischemia [35]. The accuracy of the ECG signal can be measured by the SNR, as calculated using the following formula [17]:

$$\mathrm{SNR(dB)} = 20\lg\frac{V_{\mathrm{rmsf}}}{V_{\mathrm{noise}}}, \tag{9}$$

where V_{rmsf} is the root mean square of the useful part and V_{noise} is the root mean square of the noise part.

For comparison, Table 1 and Fig. S17 (Supplementary Information) illustrate the SNR, variance σ^2, durations, and amplitudes of P, Q, R, S, and T peaks from recorded ECG curves. σ^2 is the average squared difference between the actual and expected values of the R peak. The standard SNR values obtained at I and II leads of AgCF-S dry electrodes are 27.40 and 22.66 dB, respectively. When volunteers are sitting, standing, lying, walking on a slope, walking on stairs, etc., the SNR maintains a relatively stable state at V4 lead. There are even small drops in SNR when the volunteers are squatting or walking on the ground, confirming the ability of the multilead ECG system to operate in extreme environments. For ECG curves recorded in the V4 lead, the AgCF-S dry electrode shows relatively high SNR and low σ^2 values in the above scenarios. Pure AgCF electrodes, due to their lack of adhesion, reveal low SNR and high σ^2 under large body movements. There is little difference between the durations and amplitudes of P, Q, R, S, and T peaks in the AgCF-S dry and 3M gel electrodes, whether volunteers are in static or dynamic activity. Subtle differences are caused by the physical state of volunteers, indicating that the signal and waveform obtained by AgCF-S dry electrodes are stable compared to those obtained by commercial 3M electrodes.

Table 2 summarizes the conductivity, stretchability, adhesion, and SNR of state-of-the-art ECG devices using active materials such as CNT/PDMS [45], CNT/graphene [28], graphene/silicone [18], AgNWs/polyurethane (PU) [20], AgNPs/Ecoflex [31], AgNWs/PDMS [29], zeolite-PDMS [46], MWCNT/PDMS [47], 3-(aminopropyl)triethoxysilane (APTES)-anchored PDMS [48], and Au/PDMS [49]. These works laid the foundation for the development of ECG sensing systems, but also pointed out that current ECG sensors have two limitations: (1) high SNR but limited stretchability, which is not conducive to large-scale monitoring, and (2) large strain range but low SNR, making it difficult to obtain high-fidelity signals. Compared to other cutting-edge ECG sensors, this multilead ECG system exhibits superior conductivity, high SNR, and great adhesion. The large stretchability

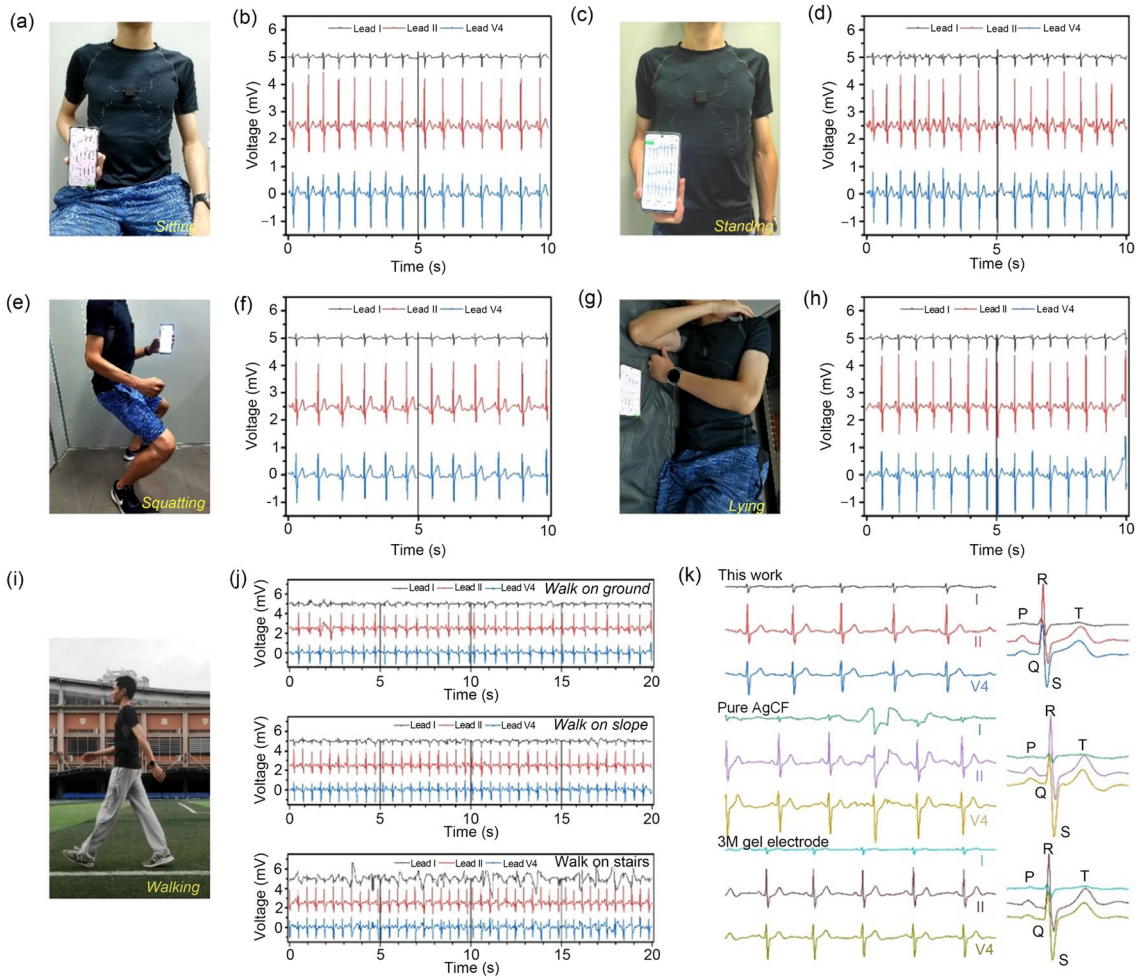

Fig. 7 Optical images of a volunteer wearing a multilead ECG device while **a**, **b** sitting, **c**, **d** standing, **e**, **f** squatting, and **g**, **h** lying to record ECG signals at I, II, and V4 leads. **i**, **j** Optical images of a volunteer wearing a multilead ECG device while walking on the ground, a slope, and stairs to record ECG signals at I, II, and V4 leads. **k** Comparison of P, Q, R, S, and T waves of AgCF-S dry electrodes with pure AgCF and 3M gel electrodes. ECG: electrocardiogram; AgCF-S: silver-coated fiber/silicone

Table 1 SNR, σ^2, duration, and amplitude of recorded ECG curves in three electrodes

	Standard	Sit	Lay	Stand	Squat	Walk on the ground	Walk on a slope	Walk on stairs
I-this-SNR (dB)	27.40	27.34	28.08	27.88	23.90	24.26	27.02	29.60
II-this-SNR (dB)	22.66	20.32	21.80	20.60	20.30	21.32	19.92	18.30
V4-this-SNR (dB)	30.54	27.56	30.62	25.60	29.20	29.00	28.28	25.24
V4-3M-SNR (dB)	30.68	28.76	31.76	27.30	28.98	30.50	29.44	30.80
V4-AgCF-SNR (dB)	30.48	28.34	29.66	28.76	29.20	34.34	28.32	25.84
V4-this-σ^2	0.04	0.08	0.04	0.07	0.08	0.07	0.09	0.10
V4-3M-σ^2	0.05	0.08	0.05	0.08	0.11	0.11	0.18	0.13
V4- AgCF-σ^2	0.11	0.10	0.08	0.11	0.21	0.23	0.41	0.18
V4-this-duration-P	0.10	0.10	0.09	0.10	0.09	0.11	0.08	0.08
V4-this-duration-QRS	0.11	0.10	0.11	0.12	0.12	0.10	0.12	0.10
V4-this-duration-T	0.20	0.16	0.21	0.19	0.18	0.18	0.18	0.15

Table 1 (continued)

	Standard	Sit	Lay	Stand	Squat	Walk on the ground	Walk on a slope	Walk on stairs
V4-3M-duration-P	0.08	0.08	0.10	0.09	0.08	0.09	0.08	0.08
V4-3M-duration-QRS	0.10	0.10	0.11	0.11	0.10	0.12	0.11	0.10
V4-3M-duration-T	0.18	0.20	0.21	0.18	0.16	0.20	0.17	0.19
V4-this-amplitude-P	0.09	0.12	0.11	0.09	0.08	0.12	0.08	0.12
V4-this-amplitude-QRS	1.78	2.03	1.69	2.08	2.12	1.90	1.97	1.96
V4-this-amplitude-T	0.26	0.23	0.28	0.27	0.32	0.26	0.26	0.29
V4-3M-amplitude-P	0.08	0.12	0.10	0.16	0.09	0.11	0.10	0.19
V4-3M-amplitude-QRS	1.96	1.98	1.98	2.20	2.23	1.97	2.01	2.17
V4-3M-amplitude-T	0.31	0.32	0.27	0.22	0.26	0.26	0.27	0.33

SNR: signal-to-noise ratio; σ^2: the variance; ECG: electrocardiogram

Table 2 Comparison of representative on-skin ECG electrodes to AgCF-S dry electrodes

	Materials	Conductivity/resistivity	Stretchability	Adhesion	SNR
Flexible/stretchable ECG electrode	This work	1.37 Ω/sq	100	0.43	15.27 vs. 15.34 dB
	CNT/PDMS	10^{-2}–10^{-1} S/cm	30	NA	NA [45]
	CNT/graphene	100 Ω/cm	100	1.3	NA [28]
	Graphene/silicone	10.96 Ω/sq	1000	NA	24.1 vs. 21.6 dB [18]
	AgNWs/PU	9190 S/cm	310	NA	24.31 vs. 24.86 dB [20]
	AgNPs/Ecoflex	9.43×10^{-5} Ω/cm	119	NA	10.57 vs. 11.05 dB [31]
	AgNWs/PDMS	35 Ω/sq	400	NA	NA [29]
Hard/nonflexible electrode	Zeolite-PDMS	0.58 μS/mm	NA	NA	42.9 dB vs. NA [46]
	MWCNT/PDMS	481–685 mS/cm	NA	NA	35.8–38.7 dB vs. NA [47]
	APTES-anchored PDMS	NA	NA	0.4	21.82 vs. 21.82 dB [48]
	Au/PDMS	NA	NA	1.2	NA [49]

ECG: electrocardiogram; AgCF-S: silver-coated fiber/silicone; SNR: signal-to-noise ratio; CNT: carbon nanotube; PDMS: polydimethylsiloxane; AgNWs: silver nanowires; AgNPs: silver nanoparticles; MWCNT: multi-walled carbon nanotube; APTES: 3-(aminopropyl)triethoxysilane; NA: not applicable

of 100% is enough to cope with various deformations in daily life.

Conclusions

This study reported the design and fabrication of on-skin stretchable and conductive AgCF-S dry electrodes for multilead ECG devices. Tangential and normal adhesion of ECG dry electrodes was tested by the self-built platform. Allergies did not occur on ECG dry electrodes after 24 h measurement on pigskin. The total weight of the multilead ECG sensing system, including clothing, ECG dry electrodes, and the core, was about 150 g, lighter than many state-of-the-art works and not burdensome for users to wear. Small intrinsic impedance and contact impedance were obtained in high-frequency vibration (about 70 Hz). Thus, the wearable ECG device could catch I–III, aVR, aVL, aVF, and V4 lead data which could be further visualized on a mobile terminal. High SNR and σ^2 values in V4 lead indicate that the wearable ECG system meets operational needs in various scenarios. The as-fabricated AgCF-S dry electrode has relatively high conductivity and SNR, which, combined with the unique advantages of wireless transmission and visualization in multilead ECG devices, determines its broad prospects in wearable electronics.

Supplementary Information The online version contains supplementary material available at https://doi.org/10.1007/s42242-023-00268-w.

Acknowledgements This study was supported by the Natural Science Foundation of Guangdong Province, China (No. 2021B1515020087), the National Natural Science Foundation of China (No. 51905178), and the Climbing Program Foundation of Guangdong Province (No. pdjh2022a0024).

Author contributions The manuscript was completed through contributions of all authors. All authors have given approval to the final version of the manuscript.

Declarations

Conflict of interest The authors declare that they have no conflict of interest.

Ethical approval Experiments involving human subjects were conducted with the full informed consent of volunteers.

References

1. Attia ZI, Kapa S, Lopez-Jimenez F et al (2019) Screening for cardiac contractile dysfunction using an artificial intelligence-enabled electrocardiogram. Nat Med 25:70–74. https://doi.org/10.1038/s41591-018-0240-2
2. Hannun AY, Rajpurkar P, Haghpanahi M et al (2019) Cardiologist-level arrhythmia detection and classification in ambulatory electrocardiograms using a deep neural network. Nat Med 25:65–69. https://doi.org/10.1038/s41591-018-0268-3
3. Takaya M, Matsuda R, Inamori G et al (2021) Transformable electrocardiograph using robust liquid–solid heteroconnector. ACS Sens 6(1):212–219. https://doi.org/10.1021/acssensors.0c02135
4. Masihi S, Panahi M, Maddipatla D et al (2021) Development of a flexible wireless ECG monitoring device with dry fabric electrodes for wearable applications. IEEE Sens J 22(12):11223–11232. https://doi.org/10.1109/JSEN.2021.3116215
5. Yang J, Zhang K, Yu JJ et al (2021) Facile fabrication of robust and reusable PDMS supported graphene dry electrodes for wearable electrocardiogram monitoring. Adv Mater Technol 6(9):2100262. https://doi.org/10.1002/admt.202100262
6. Maithani Y, Choudhuri B, Mehta BR et al (2021) Self-adhesive, stretchable, and dry silver nanorods embedded polydimethylsiloxane biopotential electrodes for electrocardiography. Sens Actuat A Phys 332:113068. https://doi.org/10.1016/j.sna.2021.113068
7. Niu X, Wang LZ, Li H et al (2022) Fructus xanthii-inspired low dynamic noise dry bioelectrodes for surface monitoring of ECG. ACS Appl Mater Interfaces 14(4):6028–6038. https://doi.org/10.1021/acsami.1c22303
8. Kota D, Tasneem N, Kakaraparty K et al (2022) A low-power dry electrode-based ECG signal acquisition with de-noising and feature extraction. J Signal Process Syst 94(6):579–593. https://doi.org/10.1007/s11265-021-01681-z
9. Lazaro J, Reljin N, Hossain MB et al (2020) Wearable armband device for daily life electrocardiogram monitoring. IEEE Trans Biomed Eng 67(12):3464–3473. https://doi.org/10.1109/TBME.2020.2987759
10. Maji S, Burke MJ (2020) Establishing the input impedance requirements of ECG recording amplifiers. IEEE Trans Instrum Meas 69(3):825–835. https://doi.org/10.1109/TIM.2019.2907038
11. Hoseini Z, Nazari M, Lee KS (2021) Current feedback instrumentation amplifier with built-in differential electrode offset cancellation loop for ECG/EEG sensing frontend. IEEE Trans Instrum Meas 70:2001911. https://doi.org/10.1109/TIM.2020.3031205
12. Kim HL, Kim MG, Lee C et al (2012) Miniaturized one-point detectable electrocardiography sensor for portable physiological monitoring systems. IEEE Sens J 12(7):2423–2424. https://doi.org/10.1109/JSEN.2012.2192260
13. Yeo WH, Kim YS, Lee J et al (2013) Multifunctional epidermal electronics printed directly onto the skin. Adv Mater 25(20):2773–2778. https://doi.org/10.1002/adma.201204426
14. Wang YY, Jiang LL, Ren L et al (2021) Towards improving the quality of electrophysiological signal recordings by using microneedle electrode arrays. IEEE Trans Biomed Eng 68(11):3327–3335. https://doi.org/10.1109/TBME.2021.3070541
15. Koo JH, Jeong S, Shim HJ et al (2017) Wearable electrocardiogram monitor using carbon nanotube electronics and color-tunable organic light-emitting diodes. ACS Nano 11(10):10032–10041. https://doi.org/10.1021/acsnano.7b04292
16. Zeng ZK, Huang Z, Leng KM et al (2020) Nonintrusive monitoring of mental fatigue status using epidermal electronic systems and machine-learning algorithms. ACS Sens 5(5):1305–1313. https://doi.org/10.1021/acssensors.9b02451
17. Zhang SP, Chhetry A, Zahed MA et al (2022) On-skin ultrathin and stretchable multifunctional sensor for smart healthcare wearables. npj Flex Electron 6(1):11. https://doi.org/10.1038/s41528-022-00140-4
18. Sun B, McCay RN, Goswami S et al (2018) Gas-permeable, multifunctional on-skin electronics based on laser-induced porous graphene and sugar-templated elastomer sponges. Adv Mater 30(50):e1804327. https://doi.org/10.1002/adma.201804327
19. Uguz DU, Canbaz ZT, Antink CH et al (2022) A novel sensor design for amplitude modulated measurement of capacitive ECG. IEEE Trans Instrum Meas 71:4000710. https://doi.org/10.1109/TIM.2022.3145401
20. Jiang Z, Nayeem MOG, Fukuda K et al (2019) Highly stretchable metallic nanowire networks reinforced by the underlying randomly distributed elastic polymer nanofibers via interfacial adhesion improvement. Adv Mater 31(37):e1903446. https://doi.org/10.1002/adma.201903446
21. Vuorinen T, Noponen K, Vehkaoja A et al (2019) Validation of printed, skin-mounted multilead electrode for ECG measurements. Adv Mater Technol 4(9):1900246. https://doi.org/10.1002/admt.201900246
22. Hong YJ, Jeong H, Cho KW et al (2019) Wearable and implantable devices for cardiovascular healthcare: from monitoring to therapy based on flexible and stretchable electronics. Adv Funct Mater 29(19):1808247. https://doi.org/10.1002/adfm.201808247
23. Shiba Y, Fernandes S, Zhu WZ et al (2012) Human ES-cell-derived cardiomyocytes electrically couple and suppress arrhythmias in injured hearts. Nature 489(7415):322–325. https://doi.org/10.1038/nature11317
24. Khoshmanesh F, Thurgood P, Pirogova E et al (2021) Wearable sensors: at the frontier of personalised health monitoring, smart prosthetics and assistive technologies. Biosens Bioelectron 176:112946. https://doi.org/10.1016/j.bios.2020.112946
25. Bauer M, Wunderlich L, Weinzierl F et al (2021) Electrochemical multi-analyte point-of-care perspiration sensors using on-chip three-dimensional graphene electrodes. Anal Bioanal Chem 413(3):763–777. https://doi.org/10.1007/s00216-020-02939-4
26. Jiang YZ, Liu LL, Chen L et al (2021) Flexible and stretchable dry active electrodes with PDMS and silver flakes for bio-potentials sensing systems. IEEE Sens J 21(10):12255–12268. https://doi.org/10.1109/JSEN.2021.3061949
27. Afroj S, Tan S, Abdelkader AM et al (2020) Highly conductive, scalable, and machine washable graphene-based e-textiles for multifunctional wearable electronic applications. Adv Funct Mater 30(23):2000293. https://doi.org/10.1002/adfm.202000293
28. Kim T, Park J, Sohn J et al (2016) Bioinspired, highly stretchable, and conductive dry adhesives based on 1D–2D hybrid carbon nanocomposites for all-in-one ECG electrodes. ACS Nano 10(4):4770–4778. https://doi.org/10.1021/acsnano.6b01355
29. Kim JH, Kim SR, Kil HJ et al (2018) Highly conformable, transparent electrodes for epidermal electronics. Nano Lett 18(7):4531–4540. https://doi.org/10.1021/acs.nanolett.8b01743
30. Chun S, Kim DW, Baik S et al (2018) Conductive and stretchable adhesive electronics with miniaturized octopus-like suckers

against dry/wet skin for biosignal monitoring. Adv Funct Mater 28(52):1805224. https://doi.org/10.1002/adfm.201805224
31. Guo W, Zheng P, Huang X et al (2019) Matrix-independent highly conductive composites for electrodes and interconnects in stretchable electronics. ACS Appl Mater Interfaces 11(8):8567–8575. https://doi.org/10.1021/acsami.8b21836
32. Jung H, Moon J, Baek D et al (2012) CNT/PDMS composite flexible dry electrodes for long-term ECG monitoring. IEEE Trans Biomed Eng 59(5):1472–1479. https://doi.org/10.1109/TBME.2012.2190288
33. Qin Q, Li JQ, Yao SS et al (2019) Electrocardiogram of a silver nanowire based dry electrode: quantitative comparison with the standard Ag/AgCl gel electrode. IEEE Access 7:20789–20800. https://doi.org/10.1109/ACCESS.2019.2897590
34. Wang WT, Lu LS, Lu XY et al (2022) Laser-induced jigsaw-like graphene structure inspired by *Oxalis corniculata* Linn. leaf. Bio-Des Manuf 5(4):700–713. https://doi.org/10.1007/s42242-022-00197-0
35. Liu CY, Zhang XY, Zhao LN et al (2019) Signal quality assessment and lightweight QRS detection for wearable ECG smartvest system. IEEE Internet Things J 6(2):1363–1374. https://doi.org/10.1109/JIOT.2018.2844090
36. Fink PL, Muhammad Sayem AS, Teay SH et al (2021) Development and wearer trial of ECG-garment with textile-based dry electrodes. Sens Actuat A Phys 328:112784. https://doi.org/10.1016/j.sna.2021.112784
37. Liu L, Li HY, Fan YJ et al (2019) Nanofiber-reinforced silver nanowires network as a robust, ultrathin, and conformable epidermal electrode for ambulatory monitoring of physiological signals. Small 15(22):e1900755. https://doi.org/10.1002/smll.201900755
38. Xu XW, Luo M, He P et al (2019) Screen printed graphene electrodes on textile for wearable electrocardiogram monitoring. Appl Phys A Mater Sci Process 125(10):714. https://doi.org/10.1007/s00339-019-3006-x
39. Wicaksono I, Tucker CI, Sun T et al (2020) A tailored, electronic textile conformable suit for large-scale spatiotemporal physiological sensing in vivo. npj Flex Electron 4(1):5. https://doi.org/10.1038/s41528-020-0068-y
40. Yokus MA, Jur JS (2016) Fabric-based wearable dry electrodes for body surface biopotential recording. IEEE Trans Biomed Eng 63(2):423–430. https://doi.org/10.1109/TBME.2015.2462312
41. Wang WT, Lu LS, Li ZH et al (2021) Fingerprint-inspired strain sensor with balanced sensitivity and strain range using laser-induced graphene. ACS Appl Mater Interfaces 14(1):1315–1325. https://doi.org/10.1021/acsami.1c16646
42. Feng B, Jiang X, Zou GS et al (2021) Nacre-inspired, liquid metal-based ultrasensitive electronic skin by spatially regulated cracking strategy. Adv Funct Mater 31(29):2102359. https://doi.org/10.1002/adfm.202102359
43. Peng S, Xu K, Chen W (2019) Comparison of active electrode materials for non-contact ECG measurement. Sensors 19(16):3585. https://doi.org/10.3390/s19163585
44. Peng S, Xu K, Bao SJ et al (2021) Flexible electrodes-based smart mattress for monitoring physiological signals of heart and autonomic nerves in a non-contact way. IEEE Sens J 21(1):6–15. https://doi.org/10.1109/JSEN.2020.3012697
45. Lee SM, Byeon HJ, Lee JH et al (2014) Self-adhesive epidermal carbon nanotube electronics for tether-free long-term continuous recording of biosignals. Sci Rep 4(1):6074. https://doi.org/10.1038/srep06074
46. Pullano SA, Kota VD, Kakaraparty K et al (2022) Optically unobtrusive zeolite-based dry electrodes for wearable ECG monitoring. IEEE Sens J 22(11):10630–10639. https://doi.org/10.1109/JSEN.2022.3169504
47. Tasneem NT, Pullano SA, Critello CD et al (2020) A low-power on-chip ECG monitoring system based on MWCNT/PDMS dry electrodes. IEEE Sens J 20(21):12799–12806. https://doi.org/10.1109/JSEN.2020.3001209
48. Meng Y, Li ZB, Chen JP (2016) A flexible dry electrode based on APTES-anchored PDMS substrate for portable ECG acquisition system. Microsyst Technol 22(8):2027–2034. https://doi.org/10.1007/s00542-015-2490-y
49. Wang LF, Liu JQ, Yang B et al (2015) Fabrication and characterization of a dry electrode integrated Gecko-inspired dry adhesive medical patch for long-term ECG measurement. Microsyst Technol 21(5):1093–1100. https://doi.org/10.1007/s00542-014-2279-4

Authors and Affiliations

Yingxi Xie[1] · Longsheng Lu[1] · Wentao Wang[2] · Huan Ma[3]

✉ Wentao Wang
wangwentao@csust.edu.cn

[1] School of Mechanical and Automotive Engineering, South China University of Technology, Guangzhou 510641, China

[2] College of Automotive and Mechanical Engineering, Changsha University of Science and Technology, Changsha 410114, China

[3] Guangdong Cardiovascular Institute, Guangdong Provincial People's Hospital, Guangzhou 510080, China